Bone Reports 21 (2024) 101758

Contents lists available at ScienceDirect

Bone Reports

journal homepage: www.elsevier.com/locate/bonr

Case Report

Healing of tumor-induced osteomalacia as assessed by high-resolution peripheral quantitative computed tomography is not similar across the skeleton in the first years following complete tumor excision☆,☆☆

Nilton Salles Rosa Neto [a,b,*], Rosa Maria Rodrigues Pereira [c,1], Emily Figueiredo Neves Yuki [c,d], Fernando Henrique Carlos de Souza [c,d], Liliam Takayama [c], Maria Inez da Silveira Carneiro [e], Luiz Guilherme Cernaglia Aureliano de Lima [e,f], Augusto Ishy [d], Alexandre José Reis Elias [d]

[a] Center for Rare and Immune Disorders, Hospital Nove de Julho, São Paulo, Brazil
[b] Universidade Santo Amaro, São Paulo, Brazil
[c] Universidade de São Paulo, São Paulo, Brazil
[d] Hospital Nove de Julho, São Paulo, Brazil
[e] Instituto do Câncer do Estado de São Paulo, São Paulo, Brazil
[f] Hospital Sírio Libanês, São Paulo, Brazil

ARTICLE INFO

Keywords:
Tumor-induced osteomalacia
Phosphaturic mesenchymal tumor
FGF-23
Phosphatonin
High-resolution peripheral quantitative computed tomography

ABSTRACT

Tumor-induced osteomalacia is caused by excessive fibroblast growth factor 23 production mainly from phosphaturic mesenchymal tumors. Surgical excision or tumor ablation are the preferred treatment. Information on bone microarchitecture parameters assessed by high-resolution peripheral quantitative computed tomography is limited. We report a woman with hypophosphatemic osteomalacia with generalized pain, weakness and recurrent fractures, and a large thoracic vertebral mass extending to the posterior mediastinum. Detailed radiologic and histopathologic evaluation revealed a phosphaturic mesenchymal tumor. Two surgeries were necessary for complete removal of the mass. Clinical symptoms improved after attaining normophosphatemia. Four-year post-surgical HR-pQCT parameters, compared to baseline, showed in the left distal radius, stable trabecular and cortical volumetric bone mineral density although below reference range. There was stability of trabecular number and thickness. Both stiffness and failure load decreased. A shift in cortical parameters was noted in year 2. In the left distal tibia, trabecular volumetric bone mineral density decreased whereas cortical volumetric bone mineral density markedly increased, as did cortical area. There was stability in the trabecular number and thickness. Both stiffness and failure load improved. Findings from HR-pQCT measurements in this patient disclosed that the healing of osteomalacia is not similar across the peripheral skeletal sites in the first years following tumor removal. Results contrasted low but stable volumetric bone mineral density in the distal radius with increase in the distal tibia at the expense of cortical bone. Our report helps further delineate the pattern of bone healing after treatment of this rare bone disorder.

1. Introduction

Tumor-induced osteomalacia (TIO), or oncogenic osteomalacia, is a rare paraneoplastic condition in which a tumor, recognized as a phosphaturic mesenchymal tumor (PMT), secretes phosphaturic factors, primarily fibroblast growth factor 23 (FGF23) (Florenzano et al., 2021; Dahir et al., 2021; Jan de Beur et al., 2023a; Minisola et al., 2023). The pathophysiology of the disease is based on FGF23 inducing renal phosphate wasting by reducing the expression of NaPi-2a (sodium-dependent phosphate transport protein 2A) and NaPi-2c (sodium-

☆ This work is dedicated to the loving memory of Professor Rosa Pereira.☆☆ Presented in part at American Society of Bone and Mineral Research 2022 Annual Congress, September 9–12, 2022, Austin, TX, USA [J Bone Miner Res 38 (Suppl. 1). Available at https://www.asbmr.org/education/AbstractDetail?aid=27d6ceea-c031-4b34-a388-7c38ba31aaf9. Accessed September 10, 2023.]

* Corresponding author at: Rua Peixoto Gomide, 527, Jardim Paulista, São Paulo, SP 01409-001, Brazil.
E-mail address: nsalles@yahoo.com (N. Salles Rosa Neto).

[1] In memoriam.

https://doi.org/10.1016/j.bonr.2024.101758
Received 23 November 2023; Received in revised form 24 March 2024; Accepted 27 March 2024
Available online 2 April 2024

dependent phosphate transport protein 2C) transporters in the proximal tubule, which in turn leads to hypophosphatemia. Furthermore, FGF23 inhibits 1,25-dihydroxyvitamin D [1,25$(OH)_2$D] synthesis by suppressing 1α-hydroxylase expression and stimulating the 24-hydroxylase conversion of 25-hydroxyvitamin D and 1,25$(OH)_2$D to inactive metabolites (Florenzano et al., 2021; Jan de Beur et al., 2023a). Clinical manifestations of chronic hypophosphatemia include rickets in children and osteomalacia in adults, who develop widespread bone pain, fractures, and muscle weakness (Takashi et al., 2021).

Surgical excision or tumor ablation are the preferred treatment options (Florenzano et al., 2021; Dahir et al., 2021; Minisola et al., 2023; Jiang et al., 2021). Complete removal of the tumor tissue leads to normalization of metabolic abnormalities and improvement of clinical symptoms (Florenzano et al., 2021; Jan de Beur et al., 2023a; Jiang et al., 2021). Biochemical parameters after successful excision are expected to show rapid normalization of serum and urine phosphorus as well as 1,25$(OH)_2$D levels (Allen and Raut, 2004). However, alkaline phosphatase (ALP) and parathyroid hormone (PTH) may increase further before recovery. In the case of unresectable or non-localizable tumors, conventional treatment with phosphate supplementation and active vitamin D analogs is recommended, or the alternative burosumab, a monoclonal antibody targeting FGF23, with also satisfactory results in improving biochemical and clinical parameters (Florenzano et al., 2021; Dahir et al., 2021; Jan de Beur et al., 2021, 2023a,b; Brandi et al., 2021).

Previous studies with TIO have reported mostly low areal bone mineral density (aBMD) as assessed by dual X-ray absorptiometry (DXA) (Zimering et al., 2005; Bhambri et al., 2006; Colangelo et al., 2020; Mendes et al., 2021). Sequential evaluation of DXA parameters after specific TIO treatment and information on bone microarchitectural parameters assessed by high-resolution peripheral quantitative computed tomography (HR-pQCT) is limited in the medical literature. HR-pQCT is a low-dose X-ray imaging technique that allows for three-dimensional assessment including the geometry, volumetric bone mineral density (vBMD) and microstructure of trabecular and cortical bone parameters in the distal radius and distal tibia for the study of skeletal fragility and fracture prediction. HR-pQCT results in TIO are mostly available for patients with overt disease (Mendes et al., 2021; Zanchetta et al., 2021; Ni et al., 2022, 2023).

Herein, we report the biochemical, histopathological, and sequential imaging, including HR-pQCT data, of a woman with hypophosphatemic osteomalacia, and a large thoracic vertebral mass extending into the posterior mediastinum. Detailed evaluation disclosed a PMT, and the patient improved after surgical resection.

2. Patient evaluation and research methods

2.1. Ethical declaration

This work was approved by Hospital Nove de Julho Ethics Review Board, São Paulo, Brazil, under number 3.519.028 on August 20th, 2019. The subject read and signed informed consent for publication. The procedures were followed in accordance with the ethical standards of the responsible committee on human experimentation and with the Helsinki Declaration of 1975, as revised in 1983.

2.2. Case report

We report a 56-year-old woman from São Paulo, Brazil who, in March 2019, was transferred to our institution at the request of a neurosurgeon for treatment of suspected recurrence of lumbar spondylodiscitis. Table 1 lists the chronology of events described in this manuscript.

2.2.1. Three years before admission

In 2016, the patient complained of spontaneous sharp pain in the left midfoot, but the general practitioner did not obtain radiographies. Soon after, she broke ribs after sneezing, and these were treated conservatively. At the time, she was referred to rheumatology because of generalized pain. A DXA was obtained in August 2016 and resulted in bone density within the normal range. In 2017, she broke another rib after sneezing. Investigation disclosed hyperphosphatasemia and the rheumatologist diagnosed her with Paget's disease. Her imaging examination revealed a proximal femoral stress fracture in the right hip (Fig. S1 – Supplementary Appendix) and trabecular bone irregularities in the left iliac, suspicious for Paget's. A bone scan was obtained but no straightforward evidence of Paget's disease was present (Fig. S2 – Supplementary Appendix). MRI of the spine revealed kyphosis and reduced vertebral height in vertebrae T4, T5, T8 and L1. Of note, an extradural expansive lesion was identified within the medullary canal, on the right side of the T8 vertebra (Fig. 1). ALP elevation was observed and nevertheless she was treated with zoledronic acid. The patient did not notice improvement in pain and no changes in ALP levels were observed.

Table 1
Chronology of events.

Year	Month	Event
2016	1st semester	Spontaneous sharp pain in the left midfoot. Fracture?
	1st semester	Rib fractures from sneezing. Conservative management
	August	DXA: normal
2017	1st semester	Rib fracture from sneezing. Conservative management
	April	Hyperphosphatasemia noted
		Paget's disease misdiagnosis
	May	Proximal femoral stress fracture in the right hip. Conservative management.
	July	Extradural expansive lesion within the medullary canal (T8 vertebra)
	October	Zoledronic acid 1st dose (Paget's misdiagnosis)
	November	T12 vertebral fracture
		DXA: normal
	December	Right femoral stress fracture progression
		Internal fixation
2018	January	T3-L2 posterior spinal fusion
		T8 tumor biopsy:
		Pathology = clear cell meningioma
		ESBL *E. coli* L2-L3 spondylodiscitis
	April	Zoledronic acid 2nd dose (Paget's misdiagnosis)
		Persistent hyperphosphatasemia noted
2019	March	Fever, malaise = Hospital Admission
		Hypophosphatemia and Hyperphosphaturia noted
		T3-iliac spinal fusion extension
		Recurrence of ESBL *E. coli* L2-L3 spondylodiscitis
		T8 tumor biopsy:
		Pathology = glomangiomatosis
	April	Elevated FGF23 noted
		PET-CT uptake at T8 tumor
		T8 tumor pathology revision
		=Mesenchymal phosphaturic tumor
	September	Mediastinal tumor surgical resection and new revision of spinal fusion (T3 fracture)
	October	Persistent elevation FGF23 noted
	November	Persistent elevation FGF23 noted
	December	PET-CT uptake at residual T8 tumor
		Neurosurgical resection of the residual tumor
		Phosphorus normalization
2020	February	C2-sacrum spinal fusion extension
2023	January	Alkaline phosphatase normalization

DXA: dual X-ray absorptiometry; ESBL: extended-spectrum beta-lactamase; FGF23: fibroblast growth factor-23; PET-CT: positron emission tomography and computed tomography.

2.2.2. 16 months before admission

In November 2017, a T12 vertebral fracture was identified. A new DXA was obtained and, again, resulted normal. In December 2017, her right femoral stress fracture progressed, and she required internal fixation.

2.2.3. 14 months before admission

In January 2018 she underwent the first spinal fusion surgery. It was

Fig. 1. Magnetic resonance image of the lateral thoracic spine demonstrating extradural expansive lesion (within the medullary canal – right side of the T8 vertebra) [arrow] and loss of vertebral height in multiple vertebrae (*).

a T3-L2 posterior spinal fusion for kyphotic deformity secondary to loss of vertebral height and wedge deformities and refractory pain. Her admission laboratory results showed that ALP was still elevated. At the time, a tumor suspected of compressing the T8 vertebra was biopsied and the anatomopathological report indicated clear cell meningioma Unfortunately, the patient developed L2-L3 spondylodiscitis (caused by extended-spectrum beta-lactamase [ESBL] *Escherichia coli*) and required a new procedure, combined with ertapenem and daptomycin for 6 weeks. In April 2018, after completing the antibiotic regimen for spondylodiscitis, she received a second dose of zoledronic acid. Again, no improvement in pain or ALP levels was seen.

2.2.4. 30 days before admission

The patient reported a 30-day history of pain in her left hip, which worsened with movement, did not radiate to her left lower limb, and was refractory to over-the-counter analgesics. She had been feeling unwell for 20 days and had a fever of up to 38.8 °C (101.8 °F) and was admitted to another hospital on suspicion of pneumonia. She received antibiotics which were later broadened due to ineffectiveness. The physicians considered that she might have a complication related to the previous episode of spondylodiscitis and contacted the surgical team who requested transfer to our hospital. She had been afebrile for 5 days prior to this admission.

2.2.5. 2019 hospital admission

At this moment, failure of the screws was identified, and a new surgical revision was indicated. Rheumatologic evaluation was sought due to the previous diagnosis of Paget's disease. Her medical history included osteoarthritis, hypertension, and hypothyroidism. She reported menarche at age 12 and surgical menopause at age 46, when she underwent partial hysterectomy and left oophorectomy. The patient is Gravida 2 Para 2. Her medication included glucosamine/chondroitin, levothyroxine, losartan. Her family history was not significant for osteoporosis or femoral fractures.

A skeletal survey was ordered, which did not disclose evidence of Paget's disease nor additional fractures. Laboratory workup as seen in Table 2 revealed normal renal function, hypocalcemia, hypophosphatemia, hyperphosphatasemia, suppression of $1,25(OH)_2D$ and a reduced TmP/GFR, compatible with renal phosphorus wasting. The possibility of acquired hypophosphatemic osteomalacia was considered and C-terminal FGF23 levels, a ^{68}Ga-DOTATATE PET-CT and a repeat biopsy of the paravertebral lesion were ordered. She was started on cholecalciferol, calcitriol, and phosphate supplementation.

The patient underwent T3-iliac spinal fusion extension and repeat disk biopsy and T8 lesion biopsy. ESBL *E. coli* spondylodiscitis was again diagnosed, and she was prescribed ertapenem but developed an allergic reaction. Treatment was switched to ceftolozane/tazobactam for 9 months and she was discharged home.

The pathology report of the second biopsy indicated glomangiomatosis (a vascular variant of glomus tumor). C-terminal FGF23 levels (ELISA) were 691 RU/ml (ref < 180). The PET-CT (April/2019) was notable for tracer uptake at the T8 lesion (Fig. 2).

A request for pathology second opinion was sought at the University of São Paulo. The histological sections (Fig. 3) stained with the hematoxylin-eosin technique revealed a hypercellular neoplasm, composed of small atypical (low cytological grade) and relatively monomorphic ovoid-small epithelioid cells, arranged in a diffuse or perivascular-pericytic arrangement in a limited mixofibrohyalinizing stroma, with frequent ectatic, irregular and branched microvasculature (so called "staghorn" pattern), and with a well-differentiated/mature adipocytic component. The immunohistochemical reactions revealed consistent positivity for ERG and CD56, which, added to the morphological and clinical context, is compatible with PMT. Her final diagnosis was tumor-induced osteomalacia.

In September 2019 she underwent video thoracoscopic mediastinal tumor surgical resection and another revision of spinal fusion because of a T3 fracture. Unfortunately, she remained hypophosphatemic after the procedure.

Subsequent C-terminal FGF levels (ELISA) were obtained and

Table 2
Results of laboratory tests in 2019 – hospital admission; two (2021), and four (2023) years after complete tumoral resection.

Parameter	2019	2021	2023	Reference range
Calcium, total, serum[a]	8.0	9.7	10.1	8.3–10.6 mg/dl
Albumin, serum[b]	2.5	–	–	3.4–4.8 g/dl
Calcium, total, corrected[c]	9.2	–	–	8.3–10.6 mg/dl
Phosphorus, serum[d]	1.1	4.1	4.2	2.5–4.8 mg/dl
Alkaline phosphatase[e]	217	133	103	46–116 U/l
Creatinine, serum[f]	0.65	0.85	0.85	0.5–1.1 mg/dl
eGFR[g]	108	83	82	≥60 ml/min/1.73 m^2
PTH[h]	64	37.7	55	12–88 pg/ml
1,25-Di-Hydroxyvitamin D[h]	<7.5	–	–	18–78 pg/ml
25-Hydroxyvitamin D[h]	25.19	65.14	48.68	30–60 ng/ml
TmP/GFR[c]	1.8	–	–	2.6–3.8 mg/dl
C-terminal FGF-23[i]	691	–	–	<180 RU/ml

PTH: parathyroid hormone; eGFR: estimated glomerular filtration rate; CKD-EPI: chronic kidney disease epidemiology collaboration; TmP/GFR: ratio of tubular maximum reabsorption of phosphate to glomerular filtration rate.

[a] Colorimetric, o-cresolphthalein complexone.
[b] Colorimetric.
[c] Formula.
[d] Colorimetric, phospho-molybidic acid.
[e] Enzymatic, para-nitrophenyl phosphate.
[f] Colorimetric, kinetic Jaffe method.
[g] CKD-EPI formula.
[h] Chemiluminescence immunoassay.
[i] ELISA.

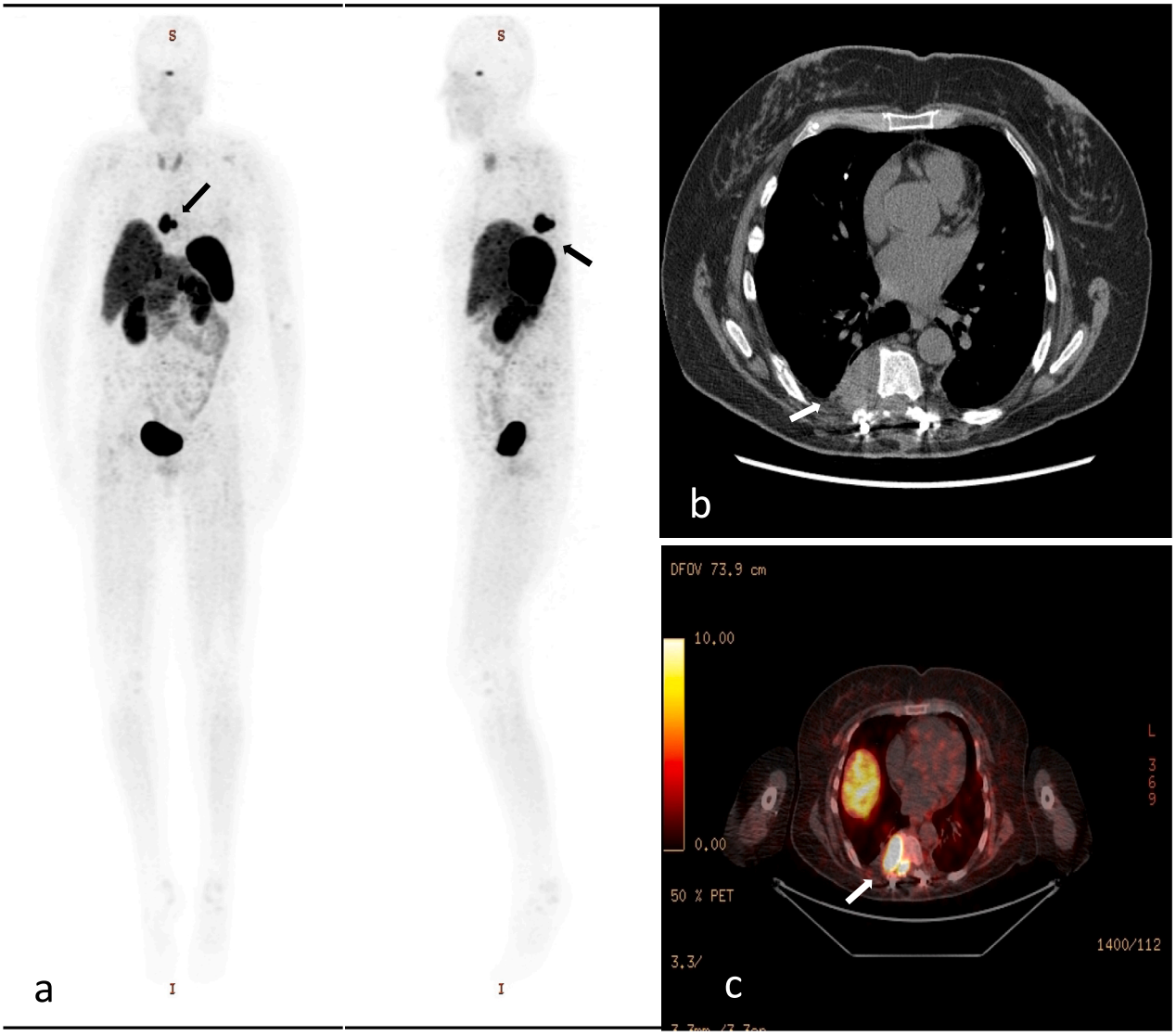

Fig. 2. Whole body ^{68}Ga-DOTATATE positron emission tomography image (April/2019) notable for tracer uptake at the T8 lesion (arrows) a) PET scan anteroposterior and lateral views, b) computed tomography transverse view and c) transverse view image fusion.

remained elevated 764 RU/ml (October) and 1564 RU/ml (November). A repeat ^{68}Ga-DOTATATE PET-CT (December) disclosed incomplete tumor resection (Fig. S3 – Supplementary Appendix). And she endured a fixed cervical deformity following the spinal surgery.

In December 2019 the patient underwent neurosurgical dorsal approach resection of the tumor. Phosphorus levels normalized in the immediate post-surgical evaluation and remain within the normal range. Pathology report was again compatible with PMT and there was no evidence of malignancy.

Biochemical parameters following successful excision show normalization of serum/urinary phosphorus levels, but elevation of ALP, PTH and 1,25$(OH)_2$D above the reference range, before recuperation. Sequential trend of serum phosphorus, ALP, PTH and 1,25$(OH)_2$D before and after the two surgical interventions (2018–2020) are shown in Fig. S4 – Supplementary Appendix.

In February 2020 she underwent another revision surgery to correct the cervical deformity, a C2-sacrum spinal fusion extension (Fig. S5 – Supplementary Appendix). Her current height is 1.54 m [5 ft. 1in] (previous height was 1.67 m [5 ft. 6in]).

As of October 2021, after a long interval at home she reported improvement in walking, absence of pain and no falls despite not having been on physical therapy because of the COVID-19 restrictions. She reported mild exertional dyspnea. The patient was still on calcitriol 0.25μg/day, cholecalciferol 2000UI/day and calcium carbonate 1 g/day as recommended after her last surgery. Given improvements in the biochemical parameters (Table 2 – 2021), calcitriol was interrupted. It can still be noted that ALP had not normalized despite the correction of all mineral abnormalities.

In January 2023, new laboratory results show ALP within the reference range alongside serum calcium, phosphorus, creatinine, 25-hydroxyvitamin D and PTH, as shown in Table 2 – 2023.

2.3. Dual-energy X-ray absorptiometry

Dual-energy X-ray absorptiometry (Prodigy, GE HealthCare Technologies Inc., Chicago, IL, USA), performed at the University of São Paulo in 2019 prior to tumor removal, showed aBMD within the normal range (T-scores > -1.0) in the left total hip and left one-third radius. Lumbar spine was not assessed because of surgical artifacts. The minimum meaningful change for the total hip is 4.4 %.

Two years after tumoral excision, DXA showed a 0.245 g/cm^2 (+29.2 %) significant increase in the left total hip. No significant changes were observed in the values for the left one-third radius in the comparative analysis between 2021 and 2019. In 2023, DXA revealed an

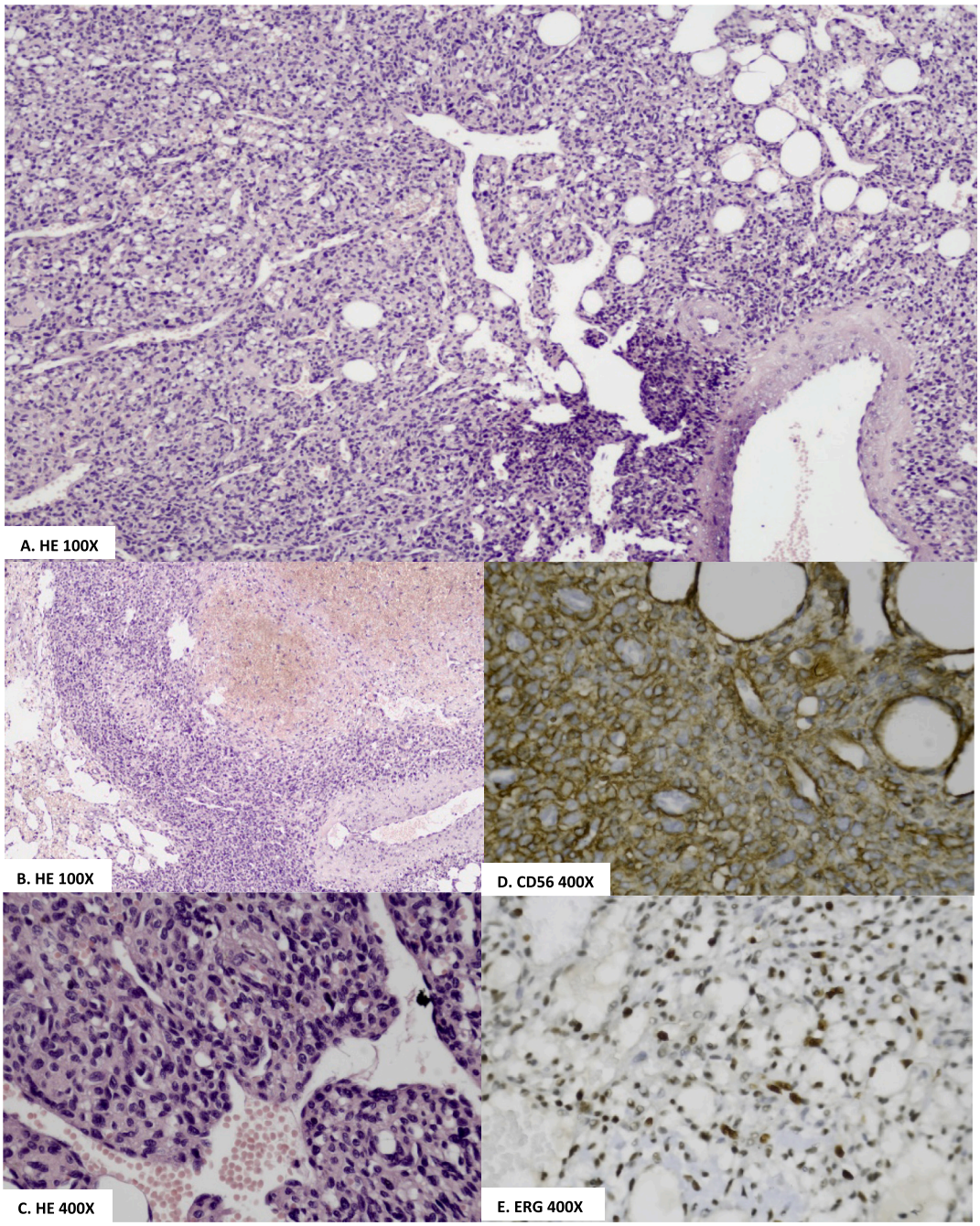

Fig. 3. Histopathological evaluation revealing phosphaturic mesenchymal tumor. A) Hematoxylin-eosin stain 100×, B) Hematoxylin-eosin stain 100×, C) Hematoxylin-eosin stain 400×, D) Immunohistochemical stain CD56 400×, E) Immunohistochemical stain ERG 400×.

additional significant increase of 0.069 g/cm^2 (+6.4 %) in the left total hip aBMD as compared to the 2021 exam. Notably, left one-third radius aBMD did not change significantly in this two-year period.

In summary, after four years of the surgical excision, aBMD significantly increased in left total hip (+37.4 %) and did not change significantly in the one-third radius. Fig. S6 – Supplementary Appendix illustrates our patient's 4-year BMD evolution.

2.4. High-resolution peripheral quantitative computed tomography imaging

High-resolution peripheral quantitative computed tomography imaging parameters (HR-pQCT; nominal resolution voxel size 82 μm; Xtreme CT Scanco Medical AG, Brüttisellen, Switzerland) were assessed at the left distal radius and the left distal tibia, also at three timepoints: 2019 before surgery, and 2021 and 2023, performed by the same technician. Regarding precision, the coefficient of variation is 0.93–1.41 % at the distal radius and 0.25–1.16 % at the tibia for density measurements, and 1.49–7.59 % at the distal radius and 0.78–6.35 % at tibia for morphometric measurements. Different trends in the radius and tibia vBMD during the four years following tumoral excision were observed.

In the left distal radius, cortical vBMD decreased significantly after two years 45.1 mg HA/cm^3 (−5.1 %) and remained stable in the next two years: +22.5 mg HA/cm^3 (+2.7 %, not significant). Trabecular vBMD as well as cortical and trabecular area remained stable throughout the four years. Of note, there was a 11,000 N/mm (−12.4 %) reduction in the radius stiffness after two years but a later 7000 N/mm (+7.8 %)

gain. Similarly, a reduction of 466 N (−11.2 %) was noted in the failure load in 2021, with a later 311 N (+8.4 %) increase.

In the left distal tibia, cortical vBMD increased significantly after two years 73 mg HA/cm^3 (+10.4 %) and remained stable in the next two years: +19.7 mg HA/cm^3 (+2.5 %, not significant). On the contrary, trabecular vBMD decreased significantly after two years 9.9 mg HA/cm^3 (−5.3 %) and remained stable in the next two years 3.2 mg HA/cm^3 (−1.6 %, not significant). Cortical area increased significantly 20.7 mm^2 (+29.2 %) after two years and later remained stable. Tibia trabecular area did not change significantly over four years. Importantly, there was a 14,000 N/mm (+8.8 %) increase in the tibia stiffness after two years, and further increase in the next two years of 5000 N/mm (+2.9 %). Similarly, an increase of 695 N (+9.3 %) was noted in the failure load in 2021, with further 29 N (+3.6 %) increase in the next two years.

In summary, after four years, in the left distal radius, trabecular and cortical vBMD, cortical area, trabecular thickness and trabecular number remained stable despite some significant shifts in between. Both stiffness and failure load decreased 4000 N/mm (−4.5 %) and 155 N (−3.7 %) respectively. In the left distal tibia, trabecular vBMD decreased 13.1 mg HA/cm^3 (−7.0 %) whereas cortical vBMD markedly increased 92.8 mg HA/cm^3 (+13.2 %). Cortical area increased 27 mm^2 (+38 %), whereas trabecular number and thickness remained stable. Both stiffness and failure load improved 19,000 N/mm (+11.9 %) and 985 N (+13.2 %) respectively. Figs. S7 and S8 and Tables S1 and S2 – Supplementary Appendix illustrate our patient's HR-pQCT parameters evolution over four years.

3. Discussion

We report a case of a woman with tumor-induced osteomalacia who was misdiagnosed with Paget's disease and received two doses of zoledronic acid, and whose tumor pathology was only diagnostic after a third examination. Eventually, she was accurately diagnosed and effectively treated with tumor excision, although requiring two surgical procedures. We present histopathological, biochemical, DXA and HR-pQCT sequential assessments or measurements showing the healing pattern of tumor-induced osteomalacia in this patient.

3.1. Histopathology

The histological diagnosis of a PMT is challenging and pathologists need to differentiate it from other mesenchymal tumors. The common histological feature of PMT is the presence of mixed cellular composition, including spindled mesenchymal cells, osteoclast-like giant multinucleated cells and adipocyte/adipocytic-like cells. The mesenchymal component usually consists of elongated-shaped cells with variable cellularity and nuclear atypia, and that can be arranged in a storiform or fascicular pattern. PMT may contain thin-walled hemangiopericytomatous vessels and hemorrhagic background that are considered an important histologic feature. The osteoclast-like giant cells can be scattered throughout the tumor tissue. There may be evidence of mineralization ("grungy" calcification) or psamoma bodies within the tumor matrix in some cases (Montanari et al., 2023; Chatterjee et al., 2021; Folpe, 2019).

The diagnostic odyssey of patients with rare disease is frequently long and challenging and several health care providers are seen before the correct diagnosis is established. A similar case of spinal mass revealing PMT, following a second biopsy, has been recently reported. Authors stated that only after pathology assessment TIO was considered, encompassing at least two years of hypophosphatemia (Sistani et al., 2022). Diagnosing PMT involves not only histological examination of the tumor tissue but a combination of clinical and imaging information, together with phosphorus and C-terminal FGF-23 measurements (Florenzano et al., 2021; Dahir et al., 2021; Jan de Beur et al., 2023a; Minisola et al., 2023). Our case highlights the importance of the communication between clinicians and pathologists to achieve an accurate diagnosis.

3.2. Biochemical parameters

Monitoring biochemical parameters is crucial to assess bone healing process in hypophosphatemic osteomalacia. Not only it depends on the correction of the underlying mineral disturbance but also on maintaining adequate levels of calcium and vitamin D intake (Jan de Beur et al., 2023a; Minisola et al., 2023). In our case, the incomplete removal of the tumor after the first surgical attempt, with persistent hypophosphatemia, reinforced the importance of complete tumor excision in the treatment of the disease. Following the second procedure, phosphorus levels rapidly corrected, what confirmed complete removal of the tumoral tissue.

Interestingly, shortly after tumor surgical removal, alkaline phosphatase levels increased higher than its already elevated values, representing accelerated mineralization process. In the same direction, 1,25 (OH)2D rapidly corrected, also with early elevation beyond upper limit of normal and then returned to the normal range. In addition, parathyroid hormone levels, which were within the normal range, increased beyond the upper limit of normal after tumor removal before returning to the normal range. This is the expected pattern of metabolic correction following adequate treatment (Kilbane et al., 2021; Bosman et al., 2022; Hacisahinogullari et al., 2023; Crotti et al., 2021).

Alkaline phosphate levels, however, remained elevated for a prolonged period even after clinical symptoms improved. Previous work with elderly patients with osteomalacia caused by vitamin D deficiency has shown that, after reaching normocalcemia with vitamin D supplementation, normalization of alkaline phosphatase levels can take a year to occur in most patients, or even longer (Allen and Raut, 2004). Of note, our patient's 25OHD levels were low at diagnosis and, despite adequate intake of calcium and supplementation of vitamin D, and, despite rapid normalization of the phosphorus levels, we observed a slow decline in ALP levels. The extended healing process correlated with the improvement in the structural parameters observed with HR-pQCT sequential exams over the four-year follow-up period. One should interpret these findings in the light of preceding two-year exposure to zoledronic acid before surgical excision of the tumor.

3.3. Dual-energy X-ray absorptiometry

Osteomalacia may or may not present with low bone density (Bosman et al., 2022; Saghafi et al., 2013). Correction of the underlying disturbance usually reflects improvement of aBMD in lumbar spine and total hip but stability or worsening in the one-third radius (Zimering et al., 2005; Bhambri et al., 2006; Colangelo et al., 2020; Mendes et al., 2021). Our patient had normal BMD measurements prior to diagnosis and, nevertheless, DXA showed increasing aBMD in total hip following tumor excision, corroborating the healing of osteomalacia. A greater increase in aBMD was observed in the first two years after surgery, but an additional significant increase in the next two years in the left total hip could be demonstrated. As expected, one-third radius aBMD remained stable over the 4-year period. These findings are in consonant with the patient's biochemical improvements and may reflect improved mineralization following normalization of phosphate levels.

3.4. HR-pQCT

There are few reports of HR-pQCT analyses in TIO. More frequently, authors present results of a single analysis, usually prior to surgery or in cases of no localization of the tumor with persistent disease (Mendes et al., 2021; Zanchetta et al., 2021; Ni et al., 2022, 2023). To the best of our knowledge, only one group reported comparative HR-pQCT results, in Chinese patients, pre- and post- surgical resection. Authors showed comparatively decreased radius cortical porosity and increased tibial cortical porosity and cortical thickness in 15 patients 1 year after

surgery. No other meaningful changes were observed in these subjects (Ni et al., 2022). The same group reported measurements of 22 patients before and 3 months after surgery, demonstrating deterioration of trabecular and cortical vBMD, and microstructure of trabecular bone (trabecular number, separation, and bone volume ratio) and cortical bone (cortical thickness and porosity) at the distal radius or tibia (Ni et al., 2023).

Our patient had remarkably higher trabecular vBMD in the left distal radius compared to age-matched healthy Brazilian women (Alvarenga et al., 2017) and it remained stable above reference range after four years. On the contrary, the patient had remarkably lower cortical vBMD in the same region which, despite a significant decrease in the first two years following surgery, the overall result depicted stability after four years. This may reflect "trabecularization" of cortical bone, but the absence of histological analysis prevents us from reaching this conclusion. The BMD loss was more pronounced in the second year after surgery and then increased in the fourth year, although remaining below reference range. Trabecular number remained above range and trabecular separation and thickness, below range. Cortical thickness started within range, fell below range on year two but returned to normal range on year four. Despite lower cortical vBMD, the stiffness and failure load measurements had numbers above range, suggesting good bone resistance before surgery, which, eventually, fell to normal range on year two, but returned to higher levels on year four.

With regards to the tibia measurements, our patient had a similar trend, of elevated trabecular vBMD with a significant loss after four years but remaining above range, and a decreased cortical vBMD, with a significant increase after four years, but still below reference range. Trabecular number remained above range and trabecular separation, below range. Trabecular thickness persisted within range. Cortical thickness was lower than reference and only on year four it normalized. Stiffness and failure load were below range before surgery, but gradually improved up to year four, suggesting adequate bone resistance according to patient's age.

A limitation of our work is the lack of bone biopsy for comparison to the noninvasive imaging. Previous study of histomorphometric measurements in adults with X-linked hypophosphatemia treated with burosumab focused on changes in iliac trabecular bone after 48-week treatment period as compared to baseline (Insogna et al., 2019). Results showed improvement in osteoid volume/total bone volume, osteoid surface/total bone surface, osteoid thickness, equivalent to healing of osteomalacia with drug therapy, but authors did not quantify the osteomalacia or its expected healing in the cortical compartment. Nevertheless authors informed increased median cortical thickness and hypothesized that this could mean enhanced cortical strength following osteomalacia healing. Our patient showed improvement in cortical thickness and cortical strength in the tibia and stability above normal in the radius as assessed by HR-pQCT. We can hypothesize that these changes also reflect improved cortical porosity of bone that was previously "trabecularized" similar to what has been described in primary hyperparathyroidism (Vu et al., 2013) and to what has been previously reported in TIO (Ni et al., 2022).

It is indeed challenging to assert the pattern of bone healing in this patient. Of note, she was diagnosed with one disorder – tumor-induced osteomalacia and was operated because of complications related to the disease even though the diagnosis came two years after the onset of the clinical symptoms. Limited mobility and weakness are part of the clinical manifestations irrespective of surgical procedures and she definitely improved after adequate treatment despite having required a very extensive spinal fixation. We cannot exclude the impact of the multiple surgeries and surgical complications on her bone health but the clinical, biochemical and densitometric improvements were compatible with reversal of osteomalacia and much of the information obtained from HR-pQCT is expected to also be related to that improvement.

These findings reflect the diverse pattern of bone healing of osteomalacia in different skeletal sites and compartments. This discrepancy may be also partially influenced by weight-bearing differences in upper and lower limbs. Patients start to improve mobility and strength with osteomalacia recovery. However, attention is required because they may still be prone to falls. She did not received steroids during the hospital admissions that we were in charge of because of her bone disease and fracture history, but was exposed to intravenous bisphosphonate twice before the formal diagnosis of TIO and we cannot exclude the lasting impact of this drug in the pattern of healing that we described. Nevertheless, the strength of our paper is the sequential HR-pQCT measurements obtained at different timepoints of the disease after adequate TIO treatment.

4. Conclusions

The rarity of tumor-induced osteomalacia, and the lack of awareness about this entity contribute to a delay in diagnosis and treatment. Clinician and pathologist awareness is important, as is effective communication between the teams. We presented sequential HR-pQCT combined with DXA and laboratory data from a patient with resolved tumor-induced osteomalacia. Our work helps further delineate the pattern of bone healing after treatment of this rare bone disorder.

CRediT authorship contribution statement

Nilton Salles Rosa Neto: Writing – review & editing, Writing – original draft, Visualization, Supervision, Resources, Project administration, Methodology, Investigation, Formal analysis, Data curation, Conceptualization. **Rosa Maria Rodrigues Pereira:** Methodology, Investigation. **Emily Figueiredo Neves Yuki:** Investigation. **Fernando Henrique Carlos de Souza:** Writing – review & editing, Investigation. **Liliam Takayama:** Writing – review & editing, Writing – original draft, Visualization, Methodology, Investigation, Data curation. **Maria Inez da Silveira Carneiro:** Investigation. **Luiz Guilherme Cernaglia Aureliano de Lima:** Writing – review & editing, Writing – original draft, Investigation. **Augusto Ishy:** Investigation. **Alexandre José Reis Elias:** Investigation.

Declaration of competing interest

NSRN received speaker's fees from Takeda Pharmaceuticals, Abbvie, Pint Pharma and Ultragenyx; and participated in advisory boards for Janssen and Takeda Pharmaceuticals; All other authors have nothing to declare.

Data availability

The data that has been used is confidential.

Appendix A. Supplementary data

Supplementary data to this article can be found online at https://doi.org/10.1016/j.bonr.2024.101758.

References

Allen, S.C., Raut, S., 2004. Biochemical recovery time scales in elderly patients with osteomalacia. J. R. Soc. Med. 97 (11), 527–530. https://doi.org/10.1177/014107680409701104.

Alvarenga, J.C., Fuller, H., Pasoto, S.G., Pereira, R.M., 2017. Age-related reference curves of volumetric bone density, structure, and biomechanical parameters adjusted for weight and height in a population of healthy women: an HR-pQCT study. Osteoporos. Int. 28 (4), 1335–1346. https://doi.org/10.1007/s00198-016-3876-0.

Bhambri, R., Naik, V., Malhotra, N., Taneja, S., Rastogi, S., Ravishanker, U., et al., 2006. Changes in bone mineral density following treatment of osteomalacia. J. Clin. Densitom. 9 (1), 120–127. https://doi.org/10.1016/j.jocd.2005.11.001.

Bosman, A., Palermo, A., Vanderhulst, J., De Beur, S.M.J., Fukumoto, S., Minisola, S., et al., 2022. Tumor-induced osteomalacia: a systematic clinical review of 895 cases. Calcif. Tissue Int. 111 (4), 367–379. https://doi.org/10.1007/s00223-022-01005-8.

Brandi, M.L., Clunie, G.P.R., Houillier, P., Jan de Beur, S.M., Minisola, S., Oheim, R., et al., 2021. Challenges in the management of tumor-induced osteomalacia (TIO). Bone 152, 116064. https://doi.org/10.1016/j.bone.2021.116064.

Chatterjee, D., Bardia, A., Pal, R., Saikia, U.N., Bhadada, S.K., Radotra, B.D., 2021. Clinical, morphological and immunohistochemical analysis of 13 cases of phosphaturic mesenchymal tumor - a holistic diagnostic approach. Ann. Diagn. Pathol. 54, 151783 https://doi.org/10.1016/j.anndiagpath.2021.151783.

Colangelo, L., Pepe, J., Nieddu, L., Sonato, C., Scillitani, A., Diacinti, D., et al., 2020. Long-term bone mineral density changes after surgical cure of patients with tumor-induced osteomalacia. Osteoporos. Int. 31 (7), 1383–1387. https://doi.org/10.1007/s00198-020-05369-1.

Crotti, C., Bartoli, F., Coletto, L.A., Manara, M., Marini, E., Daolio, P.A., et al., 2021. Tumor induced osteomalacia: a single center experience on 17 patients. Bone 152, 116077. https://doi.org/10.1016/j.bone.2021.116077.

Dahir, K., Zanchetta, M.B., Stanciu, I., Robinson, C., Lee, J.Y., Dhaliwal, R., et al., 2021. Diagnosis and management of tumor-induced osteomalacia: perspectives from clinical experience. J. Endocr. Soc. 5 (9), bvab099 https://doi.org/10.1210/jendso/bvab099.

Florenzano, P., Hartley, I.R., Jimenez, M., Roszko, K., Gafni, R.I., Collins, M.T., 2021. Tumor-induced osteomalacia. Calcif. Tissue Int. 108 (1), 128–142. https://doi.org/10.1007/s00223-020-00691-6.

Folpe, A.L., 2019. Phosphaturic mesenchymal tumors: a review and update. Semin. Diagn. Pathol. 36 (4), 260–268. https://doi.org/10.1053/j.semdp.2019.07.002.

Hacisahinogullari, H., Tekin, S., Tanrikulu, S., Saribeyliler, G., Yalin, G.Y., Bilgic, B., et al., 2023. Diagnosis and management of tumor-induced osteomalacia: a single center experience. Endocrine 82 (2), 427–434. https://doi.org/10.1007/s12020-023-03450-3.

Insogna, K.L., Rauch, F., Kamenický, P., Ito, N., Kubota, T., Nakamura, A., et al., 2019. Burosumab improved histomorphometric measures of osteomalacia in adults with X-linked hypophosphatemia: a phase 3, single-arm, international trial. J. Bone Miner. Res. 34 (12), 2183–2191. https://doi.org/10.1002/jbmr.3843.

Jan de Beur, S.M., Miller, P.D., Weber, T.J., Peacock, M., Insogna, K., Kumar, R., et al., 2021. Burosumab for the treatment of tumor-induced osteomalacia. J. Bone Miner. Res. 36 (4), 627–635. https://doi.org/10.1002/jbmr.4233.

Jan de Beur, S.M., Minisola, S., Xia, W.B., Abrahamsen, B., Body, J.J., Brandi, M.L., et al., 2023a. Global guidance for the recognition, diagnosis, and management of tumor-induced osteomalacia. J. Intern. Med. 293 (3), 309–328. https://doi.org/10.1111/joim.13593.

Jan de Beur, S.M., Cimms, T., Nixon, A., Theodore-Oklota, C., Luca, D., Roberts, M.S., et al., 2023 Aug 14. Burosumab improves patient-reported outcomes in adults with tumor-induced osteomalacia: mixed-methods analysis. J. Bone Miner. Res. https://doi.org/10.1002/jbmr.4900 (Epub ahead of print).

Jiang, Y., Li, X., Huo, L., Liu, Y., Lyu, W., Zhou, L., et al., 2021. Chinese Society of Osteoporosis and Bone Mineral Research and Chinese Society of Endocrinology. Consensus on clinical management of tumor-induced osteomalacia. Chin. Med. J. 134 (11), 1264–1266. https://doi.org/10.1097/CM9.0000000000001448.

Kilbane, M.T., Crowley, R., Heffernan, E., D'Arcy, C., O'Toole, G., Twomey, P.J., MJ, McKenna, 2021. High bone turnover and hyperparathyroidism after surgery for tumor-induced osteomalacia: a case series. Bone Rep. 15, 101142 https://doi.org/10.1016/j.bonr.2021.101142.

Mendes, D.A.B., Coelho, M.C.A., Gehrke, B., de Pinho, L.K.J., Cardoso Lima, L.F., Paranhos-Neto, F., et al., 2021. Microarchitectural parameters and bone mineral density in patients with tumour-induced osteomalacia by HR-pQCT and DXA. Clin. Endocrinol. 95 (4), 587–594. https://doi.org/10.1111/cen.14533.

Minisola, S., Fukumoto, S., Xia, W., Corsi, A., Colangelo, L., Scillitani, A., et al., 2023. Tumor-induced osteomalacia: a comprehensive review. Endocr. Rev. 44 (2), 323–353. https://doi.org/10.1210/endrev/bnac026.

Montanari, A., Pirini, M.G., Lotrecchiano, L., Di Prinzio, L., Zavatta, G., 2023. Phosphaturic mesenchymal tumors with or without phosphate metabolism derangements. Curr. Oncol. 30 (8), 7478–7488.

Ni, X., Feng, Y., Guan, W., Chi, Y., Li, X., Gong, Y., et al., 2022. Bone impairment in a large cohort of Chinese patients with tumor-induced osteomalacia assessed by HR-pQCT and TBS. J. Bone Miner. Res. 37 (3), 454–464. https://doi.org/10.1002/jbmr.4476.

Ni, X., Zhang, Z., Guan, W., Chi, Y., Li, X., Gong, Y., et al., 2023. Shift in calcium from peripheral bone to axial bone after tumor resection in patients with tumor-induced osteomalacia. J. Clin. Endocrinol. Metab. 108 (11), e1365–e1373. https://doi.org/10.1210/clinem/dgad252.

Saghafi, M., Azarian, A., Hashemzadeh, K., Sahebari, M., Rezaieyazdi, Z., 2013. Bone densitometry in patients with osteomalacia: is it valuable? Clin. Cases Miner. Bone Metab. 10 (3), 180–182. https://doi.org/10.1016/j.bone.2021.116077.

Sistani, G., Sallam, Y., Ng, W.P., Leung, A.E., Ang, L.C., Sharma, M., 2022. Spinal intradural phosphaturic mesenchymal tumor. Can. J. Neurol. Sci. 49 (1), 120–122. https://doi.org/10.1017/cjn.2021.44.

Takashi, Y., Kawanami, D., Fukumoto, S., 2021. FGF23 and Hypophosphatemic rickets/osteomalacia. Curr. Osteoporos. Rep. 19 (6), 669–675. https://doi.org/10.1007/s11914-021-00709-4.

Vu, T.D., Wang, X.F., Wang, Q., Cusano, N.E., Irani, D., Silva, B.C., et al., 2013. New insights into the effects of primary hyperparathyroidism on the cortical and trabecular compartments of bone. Bone 55 (1), 57–63. https://doi.org/10.1016/j.bone.2013.03.009.

Zanchetta, M.B., Jerkovich, F., Nuñez, S., Mocarbel, Y., Pignatta, A., Elías, N., et al., 2021. Impaired bone microarchitecture and strength in patients with tumor-induced osteomalacia. J. Bone Miner. Res. 36 (8), 1502–1509. https://doi.org/10.1002/jbmr.4325.

Zimering, M.B., Caldarella, F.A., White, K.E., Econs, M.J., 2005. Persistent tumor-induced osteomalacia confirmed by elevated postoperative levels of serum fibroblast growth factor-23 and 5-year follow-up of bone density changes. Endocr. Pract. 11 (2), 108–114. https://doi.org/10.4158/EP.11.2.108.